Solar Energy Materials and Solar Cells 176 (2018) 397–404

Contents lists available at ScienceDirect

Solar Energy Materials and Solar Cells

journal homepage: www.elsevier.com/locate/solmat

Analysing impact of oxygen and water exposure on roll-coated organic solar cell performance using impedance spectroscopy

B. Arredondo[a,b,*], B. Romero[a], M.J. Beliatis[c], G. del Pozo[a], D. Martín-Martín[a], J.C. Blakesley[b], G. Dibb[b], F.C. Krebs[c], S.A. Gevorgyan[c], F.A. Castro[b]

[a] Área de Tecnología Electrónica, Universidad Rey Juan Carlos, C/ Tulipán s/n, 28933 Móstoles, Spain
[b] National Physical Laboratory, Hampton Rd, Teddington TW11 0LW, UK
[c] Department of Energy Conversion and Storage, Technical University of Denmark, Frederiksborgvej 399, DK-4000 Roskilde, Denmark

ARTICLE INFO

Keywords:
Organic solar cells
Degradation
Impedance spectroscopy
Roll coated OPV

ABSTRACT

In this work we study the degradation of roll-coated flexible inverted organic solar cells in different atmospheres. We demonstrate that impedance spectroscopy is a powerful tool for elucidating degradation mechanisms; it is used here to distinguish the different degradation mechanisms due to water and oxygen. Identical cells were exposed to different accelerated degradation environments using water only, oxygen only, and both water and oxygen simultaneously, all of them enhanced with UV light. The photocurrent is dramatically reduced in the oxygen-degraded samples. Impedance measurements indicate that this phenomenon is attributed to defects introduced by absorption of oxygen, which results in an increase of the acceptor impurity (N_A) at the cathode interface obtained from a Mott-Schottky analysis. Simultaneously, at the anode interface where PEDOT:PSS is not shielded by the substrate, the nature of degradation differs for the water and oxygen degraded samples. While oxygen + UV light decreases the conductivity of the PEDOT:PSS layer, water + UV light changes the PEDOT:PSS work function inducing a depletion region at the anode.

1. Introduction

Organic photovoltaics (OPV) present several advantages such as lightness, thinness and flexibility [1,2]. Moreover, the active layer can be deposited onto flexible substrates by solution process techniques, allowing low-cost manufacturing processes such as roll-to-roll (R2R) printing for large areas [3–6]. However, OPV technology is limited by reduced power conversion efficiency (PCE) compared to inorganic cells [7]. Moreover, OPV suffers from degradation due to atmospheric agents such as water and oxygen, whose effects are enhanced under illumination [8–11]. In the last years, several groups have been devoted to study the effect of these degrading agents, not only in OPV, but also in dye sensitized solar cells [12,13] and in perovskite solar cells [14,15]. Simultaneously, there has been a great effort to developed robust encapsulation techniques and coatings to prevent degradation in oxygen and water atmospheres, including photopolymerized fluorinated coatings and hybrid coatings [16–18].

The degradation of photovoltaic performance relies on the interplay between interface and active layer degradation. Earlier stability studies have shown that device degradation in air is dominated either by the photo-oxidation of the active material under illumination [19–22] or by degradation of the interface with the electrodes [10,23,24]. Furthermore, poly(3,4-ethylenedioxythiophene) polystyrene sulfonate (PEDOT:PSS) is widely used as a selective contact in OPVs. The hygroscopic nature of this transport layer makes it particularly sensitive to water and oxygen [25–27], promoting the absorption of water and thus enhancing device degradation.

Extensive work has been performed in studying OPV degradation mechanisms using different characterization techniques such as imaging techniques [28], time of flight secondary-ion mass spectrometry (TOF-SIMS) [29], characterization according to ISOS-3 protocols under different illumination conditions (accelerated full sun simulation, low level indoor fluorescent lighting, and dark storage with daily measurement under full sun simulation) [30] and incident photon-to-electron conversion efficiency (IPCE) [31]. Impedance spectroscopy (IS) has been extensively used to study organic solar cell performance, although its use to study degradation has not been widespread. The aim of this work is to study the effect of oxygen and water in the degradation of roll-coated processed inverted organic solar cells by means of IS.

We present a study of an inverted OPV based on salen-based fluorine polymer (FSP1) [32] blended with phenyl-C_{61}-butyric acid methyl ester (PCBM) on a polyethylene terephthalate (PET) substrate

* Correspondence to: Universidad Rey Juan Carlos (Edificio Departamental II, despacho 158), C/ Tulipán s/n, 28933 Móstoles, Madrid, Spain.
E-mail address: belen.arredondo@urjc.es (B. Arredondo).

http://dx.doi.org/10.1016/j.solmat.2017.10.028
Received 14 July 2017; Received in revised form 28 September 2017; Accepted 25 October 2017
Available online 07 November 2017
0927-0248/

with structure PET/Ag/PEDOT:PSS/ZnO/FSP1:PCBM/PEDOT:PSS/Ag when exposed to most critical degradation agents: water, oxygen, and water + oxygen, combined with UV light exposure. The structure is designed to be low-cost by not employing indium-tin oxide (ITO), while both the Ag layers are in the form of open grids and consequently do not block the exchange of gas between the active layers and the atmosphere. This structure therefore experiences different degradation mechanisms to other common device structures. Impedance measurements together with equivalent-circuit analysis and simulation are employed to gain insight of kinetics and energetic processes governing the device performance. Moreover, by means of IS analysis, bulk and interfacial degradation mechanisms are elucidated when exposing the sample to different environments [33–36]. Furthermore, we find good agreement between the analysis of small-signal circuital parameters extracted from impedance, the fit of the J-V curve using DC circuits, and numerical simulations of band diagrams and J-V curves using the commercial software Silvaco TCAD.

2. Experimental methods

Devices were fabricated at the Technical University of Denmark and characterised at the National Physical Laboratory. The devices were fabricated on a mini roll coater using a slot-die head for the coating of photoactive layer (FSP1:PCBM) and PEDOT:PSS while a single roll flexography was used for the deposition of Ag back electrode. Active layer thickness is t = 400 nm. Further details on the fabrication process can be found at previous work described in reference [37].

J-V curves and Cole-Cole spectra were measured with a Modulab XM series Electrochemical System. A Xe-lamp based solar simulator (conforming to IEC 60904 9:2007 class AAA) and a custom-made LED system were used for illumination. The latter comprises multiple UV and visible LEDs and is used to provide controllable irradiance while minimising sample heating.

Three nominally identical samples from the same batch were subjected to three different accelerated degradation processes. The studies were performed on unencapsulated devices to execute highly-controlled accelerated aging without the variability that naturally comes from encapsulation. To achieve this, samples were degraded and characterised employing unique portable climate chambers capable of maintaining leak/outgassing rates of < 1 ppm/h for oxygen and water. The three degradation conditions were oxygen (1% O_2), water (0.2% H_2O) and oxygen + water (1% O_2 + 0.2% H_2O) at ambient pressure in a balance gas of purified nitrogen. These low concentrations relative to air were designed to simulate the gradual exposure to contamination, and have been found to produce quantifiable and reproducible degradation on a convenient timescale. Samples were exposed to these conditions for 6 days under UV–vis LED irradiation with a UV (< 400 nm) content of 46 ± 5 W/m^2 centred at 380 nm. At all other times, samples were stored, transported and characterised under controlled conditions with maximum permitted oxygen and humidity of 100 ppm. Such precautions are necessary as very low concentrations of oxygen and humidity in the presence of light can cause both transient and permanent changes to device characteristics [38]. A control sample (fresh) was stored in inert conditions for the sake of comparison. Impedance spectra were recorded by applying a small voltage perturbation (20 mV rms) at a frequency ranging from 1 MHz to 1 Hz in dark and light conditions for voltages varying from −1 V up to 1 V. Illuminated measurements were performed at 1 sun (AM 1.5G, 1000 W/m^2) using the solar simulator and variable irradiance from 0.05 sun up to 1.5 sun equivalent using the LED system under open-circuit conditions.

3. Results and discussion

Fig. 1 shows the current density *vs*. voltage (J-V) characteristics under 1 sun illumination for the three degraded and one fresh samples.

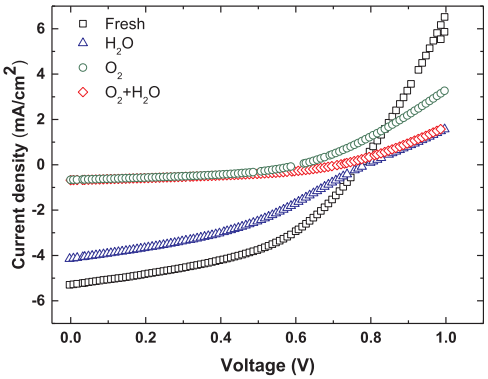

Fig. 1. Experimental J-V characteristics under AM1.5G illumination of fresh and degraded samples in different atmospheres: H_2O, O_2 and O_2 + H_2O (all combined with UV light). Device area = 1 cm^2.

Since the conductivity of ZnO can be changed with exposure to UV light, all samples were pre-treated with UV irradiation for 1 h before characterizing in order to maximize power conversion efficiency [8]. The J-V curves of the degraded samples show a decrease in the short circuit current (J_{SC}) and open circuit voltage (V_{OC}) compared to the fresh sample, as expected. Particularly, the curves exhibit a large decrease of J_{SC} for the samples that have been exposed to oxygen (O_2 and O_2 + H_2O) compared to the sample that has been exposed only to water (H_2O), in agreement with previous results found by other authors [33]. Moreover, the J-V curve of the (H_2O) sample exhibits the well-studied S-shape that results in a decrease of the fill-factor (FF) [39–41]. This S-shape is not visible, at least in the fourth quadrant of the J-V curve, for the oxygen exposed samples (O_2 and O_2 + H_2O). Table 1 summarizes the DC cell performance parameters.

These differences in the J-V behaviour of samples degraded in different atmospheres suggest that different underlying physical mechanisms are taking place and will be discussed later in the article.

Fig. 2 shows V_{OC} versus light intensity for the differently degraded samples. The ideality factor of each cell can be obtained from the slope of the linear fit. In the case of the H_2O + O_2 aged sample, the change of the slope at low light intensity may suggests a shunt resistance, so the ideality factor was calculated avoiding these low light intensities. Similar ideality factors can also be obtained from the dark J-V curves, however by using the measurements at open circuit conditions the effect of the series resistance has been avoided. Results are shown in Table 2.

It is apparent from the comparison of the slopes of all samples that those that have been exposed to oxygen (O_2 and O_2 + H_2O) exhibit a higher ideality factor. This result again suggests that the dynamical mechanisms taking place in the oxygen-degraded samples differ from those occurring in samples exposed to water. Previous theoretical and experimental investigations have linked high ideality factors to the formation of charge traps or shunts [42–45].

In order to gain a deeper insight of the physical mechanisms governing the device, we analyse the dark impedance data using a Mott-Schottky analysis at reverse and low forward bias when no significant charge is injected. For sufficiently thick samples, Mott-Schottky analysis gives information about the flat-band potential (V_{fb}) and acceptor impurity density (N_A) in the region of the metal cathode. The technique is

Table 1
Photovoltaic parameters of degraded and fresh cell under AM1.5G illumination.

	Fresh	H_2O	O_2	H_2O + O_2
V_{OC} (V)	0.71	0.63	0.59	0.63
I_{sc} (mA)	5.3	4.13	0.66	0.67
FF (%)	45.8	39	41.3	41.4
P_{max} (mW)	1.89	1.24	0.17	0.2

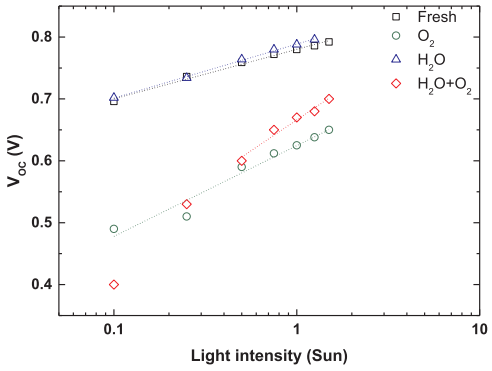

Fig. 2. Open circuit voltage versus light intensity for the different degraded samples. Ideality factor is obtained from the slope m as $n = \frac{mq}{K_B T}$. The small difference in V_{OC} values with those shown in Table 1 are due to the different illumination systems.

Table 2
Ideality factors obtained from the fits shown in Fig. 2 for different degraded samples.

	Fresh	H_2O	O_2	H_2O + O_2
n	1.34	1.46	2.46	3.4

only sensitive to doping in the contact depletion region, and is unable to confirm whether the doping is confined to one contact, or is distributed throughout the polymer. According to Kirchatz at al. [46], for devices thicker than 100 nm the determination of the doping density from the Mott−Schottky analysis becomes reliable even with low doping concentrations $N_A \sim 10^{16}$ cm^{-3}. The overall capacitance has been extracted from the Cole-Cole curves in dark condition at reverse and low forward bias. This capacitance is attributed to the depletion region due to the band bending at the cathode contact and follows a voltage dependence according to the Mott-Schottky expression [47],

$$C^{-2} = \frac{2(V_{fb} - V)}{A^2 q \varepsilon \varepsilon_0 N_A} \quad (1)$$

where V_{fb} is the flat-band potential at the cathode, N_A is the acceptor impurity density, A is the area (~ 1 cm^2), V the applied voltage, ε and ε_0 are the dielectric constant and vacuum permittivity respectively The dielectric constant is estimated from the geometrical capacitance $\left(\varepsilon = \frac{C t}{A \varepsilon_0}\right)$ at negative voltages with active layer thickness t = 400 nm, leading to values around ε = 3.5–4 for all the samples. Fig. 3 shows the fit of the capacitance using Eq. (1). This figure shows that the capacitance of the oxygen-degraded samples (O_2 and O_2 + H_2O) is one order of magnitude higher than the samples degraded in a humid atmosphere (H_2O) indicating a larger N_A for the oxygen-exposed samples (O_2 and O_2 + H_2O). Previous studies have observed that ZnO surfaces are expected to incorporate oxygen easily when exposed to oxygen

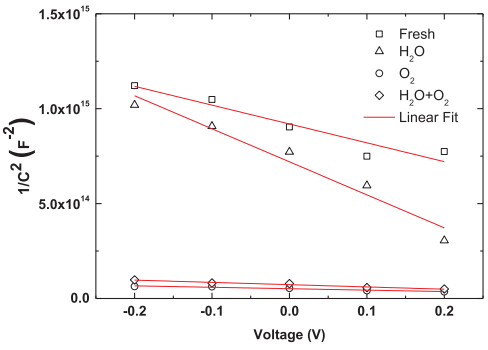

Fig. 3. Mott-Schottky fit of Eq. (1) using the capacitance extracted from the impedance measured in dark conditions versus bias voltage.

Table 3
Flat band potential, acceptor impurity density and width of the depletion region at low voltages obtained from the fit shown in Fig. 4 for all samples.

	Fresh	H_2O	O_2	H_2O + O_2
V_{fb} (V)	0.73	0.63	0.59	0.63
N_A(cm^{-3})	2.95 × 10^{16}	3.33 × 10^{16}	3.94 × 10^{17}	3.07 × 10^{17}
W(nm)	100	85	26	30

atmosphere [10], while this process is partially reversed by UV light exposure in air and almost completely reversed by UV light exposure in vacuum [48,49]. In this work, degradation was performed by exposing the samples for six days to a dilute O_2 atmosphere and UV light simultaneously. Whereas *a priori* one would expect both processes, oxygen absorption/deabsorption to compete concurrently, the increase of N_A observed empirically lead us to conclude that there is in fact a net incorporation of oxygen into the sample. This larger N_A could in turn result in the formation of additional trapping centres throughout the junction depletion region in the polymer, in agreement with the high values obtained for the ideality factors of the oxygen-degraded samples (O_2 and O_2 + H_2O).

Moreover, the capacitance-voltage measurement in the Mott-Schottky context provides a direct estimation of the width of the depletion zone according to Eq. (2). Table 3 summarises these data from the Mott-Schottky analysis.

$$W = \frac{A}{\varepsilon_r \varepsilon_0 C} \quad (2)$$

Dibb *et al.* concluded by means of numerical simulations that charge collection in the drift-driven space charge region is more efficient than charge collection by diffusion in neutral regions [50]. Moreover, in the neutral regions the recombination of minority carriers increases with the doping level, contributing to the loss in photocurrent [51]. In this context, the lower J_{sc} presented by the oxygen-degraded samples (O_2 and O_2 + H_2O) can be attributed to a less efficient charge collection due to a thinner high field depletion region (around 25 nm at short-circuit). In addition, the neutral region width (where charge collection by diffusion is not efficient) increases in the oxygen-degraded samples compared to the fresh sample, resulting in higher recombination. In contrast, water-degraded samples (H_2O) with depletion width around 100 nm exhibit a higher J_{sc}, with no significant difference compared to the fresh samples.

We can conclude that the increase of N_A in the oxygen exposed samples worsens the carrier drift driven transport and charge extraction, while the photocurrent of the water degraded cell remains almost unchanged with respect to the fresh sample.

This is in agreement with previous results using spectroscopy techniques obtained by Krebs *et al.* concluding that inverted devices fabricated with R2R were more sensitive to oxygen while standard device structures were more sensitive to water [52].

Fig. 4 shows the impedance spectra in dark conditions from 1 Hz up to 1 MHz for the fresh and degraded samples at different biases around the open circuit voltage. Symbols show the experimental data and solid lines correspond to the fit using circuit A of Fig. 5. This circuit is composed of a series resistance R_s modelling ohmic losses at contacts and wires, recombination resistance R_1, transport resistance R_2, geometrical capacitance C_2 and a constant phase element (CPE) C_1 with $Z_{CPE} = \frac{1}{(CPE_T)(i\omega)^{(CPE_P)}}$ that models a non-ideal chemical capacitance due to injected charges in the active layer. Since most of our simulations result in CPE_P ranging from 0.9 up to 1, CPE approximates to a capacitor with CPE_T being the capacitance value C_1. All samples show a high frequency arc modelling the carrier diffusion transport attributed to the unusually large active layer thickness, t = 400 nm. This high frequency feature is associated to the diffusion time defined as $\tau_d = R_2 C_1$. The circuit A of Fig. 5 fits accurately to the impedance of fresh samples, with

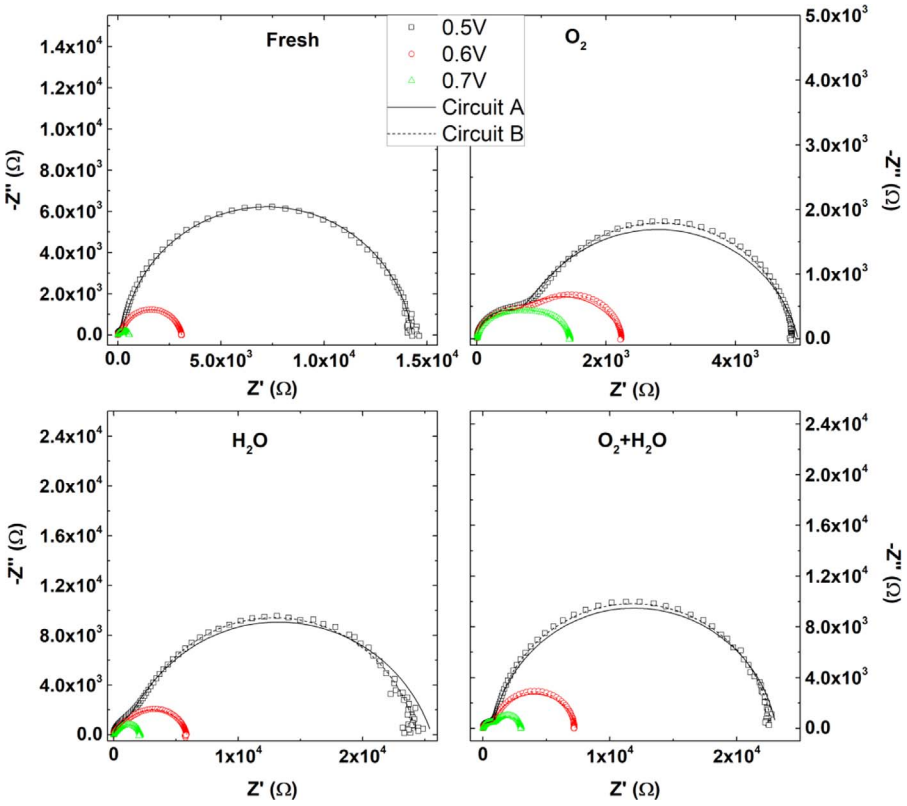

Fig. 4. Impedance spectra under dark conditions at different voltages. Solid and dashed lines show the fit to circuits A and B of Fig. 5 respectively.

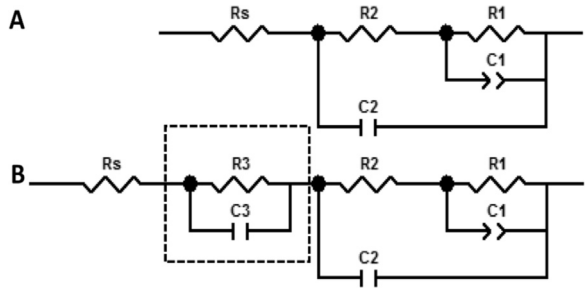

Fig. 5. Equivalent circuits used to fit impedance spectra of Fig. 4.

the low-medium frequency arc related to the recombination mechanism and its associated time defined as $\tau_{rec} = R_1 C_1$. However, circuit A does not provide good fits in the low-medium frequency arc for the oxygen and water exposed-samples. In order to obtain more accurate fits of the degraded samples, we propose to include an extra R_3C_3 displayed in circuit B of Fig. 5 and shown as dashed lines in Fig. 4. The behaviour of these additional parameters will provide important information on the nature of degradation mechanisms in the different samples.

Fig. 6 shows the voltage dependence of the parameters obtained from the fit of circuits A and B to impedance data of fresh and degraded samples, respectively, in dark conditions. Recombination resistance R_1 decreases with voltage as expected. Moreover, we find that this resistance decreases several orders of magnitude when it is obtained from impedance data under illumination (R_1~2600 Ω for the oxygen degraded samples (O_2), and R_1~500 Ω for the fresh and water exposed (H_2O) sample at zero bias), which is attributed to an increase of photogenerated carriers indicating that R_1 is associated to the organic active layer. Transport resistance R_2 also decreases with voltage and exhibits a larger value for the water only (H_2O) degraded sample, indicating that carrier diffusion is limiting transport in this sample [36]. Chemical capacitance C_1 increases with injected charge as voltage increases, while the geometrical C_2 capacitance remains almost constant.

Regarding the additional parameters included in circuit B, samples exposed to oxygen exhibit values of R_3 and C_3 that remain almost constant (C_3 slightly decreasing) with voltage. However, R_3 and C_3 for the water degraded samples vary significantly, R_3 decreasing and C_3 increasing with voltage. These differences in the parameters voltage dependence of the oxygen and only water degraded samples again indicate that different physical mechanisms are taking place. Previous studies with similar inverted device structures concluded that the degradation of the PEDOT:PSS layer is the main cause of device failure [10]. Further works have also concluded that the increase of the sheet resistance of the PEDOT:PSS even in encapsulated samples is the main cause governing the degradation of the cell upon UV exposure, and that the increase of the PEDOT:PSS resistance was found to be accelerated drastically for unencapsulated devices [53]. In this study, PEDOT:PSS is present in both contacts, however the cathode (PEDOT/ZnO) is shielded by the PET substrate while the anode was directly exposed to the degradation agents. In this context, authors believe that R_3C_3 is more likely to be associated to a degradation mechanism occurring at the anode. In the case of the oxygen degraded sample (O_2), the appearance of bias independent R_3 suggests a decrease of conductivity of the PEDOT:PSS layer at the anode with respect to the fresh sample. Moreover, if the PEDOT:PSS conductivity decreases, charges may be accumulated at this contact since they are less efficiently transferred resulting in an additional capacitance layer modelled by C_3 [10]. Both parameters, R_3 and C_3, do not significantly change with voltage. However, in the case of the water only degraded sample, both R_3 and C_3 vary with bias, suggesting that the nature of the degradation differs from a simple increase of PEDOT:PSS resistivity. In a previous study, Koch *et al.* show that residual water in PEDOT:PSS leads to a reduction of the work function due to an induced dipole formation [27]. Moreover, Norman *et al.* argue in the same direction suggesting that when PEDOT:PSS is exposed to humidity, reorganization of molecules at the interface may change the effective work function by the formation of a dipole layer at the PEDOT:PSS/active layer interface [10]. In this work, the fact that R_3 and C_3 decrease and increase with bias, respectively,

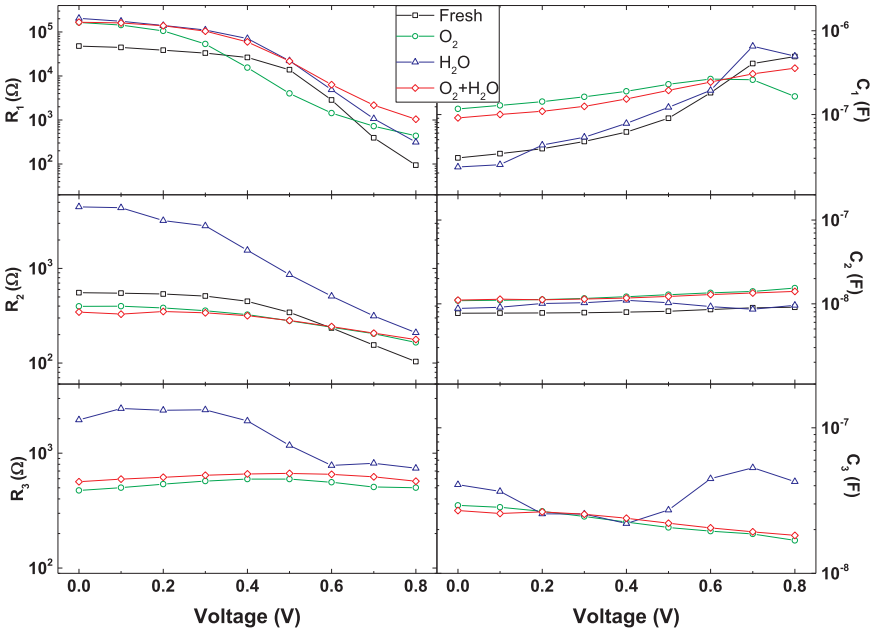

Fig. 6. Evolution of circuit parameters with bias voltage obtained from the fit of impedance data in dark conditions.

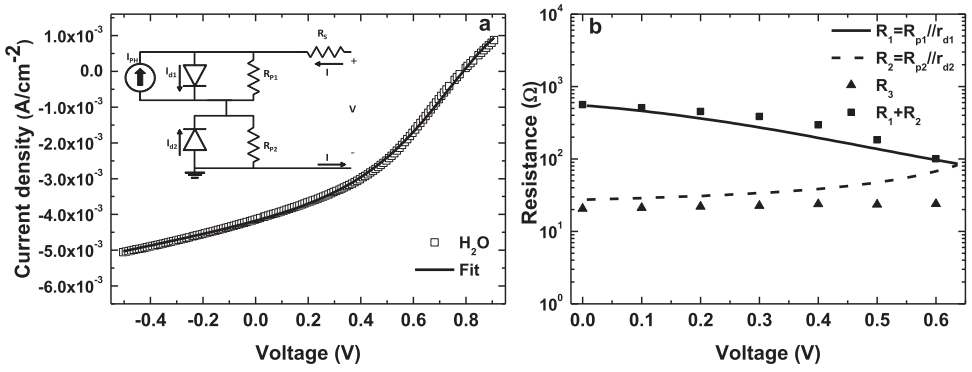

Fig. 7. a) J-V curve under 1 sun illumination AM1.5G of the water-degraded sample (symbols) and fit using the circuit of the inset (solid lines). b) Comparison of resistances obtained from the fit of the impedance spectra at 1 Sun using circuit B in Fig. 5 and resistances obtained from the fit of the J-V at 1 sun using DC circuit of the inset.

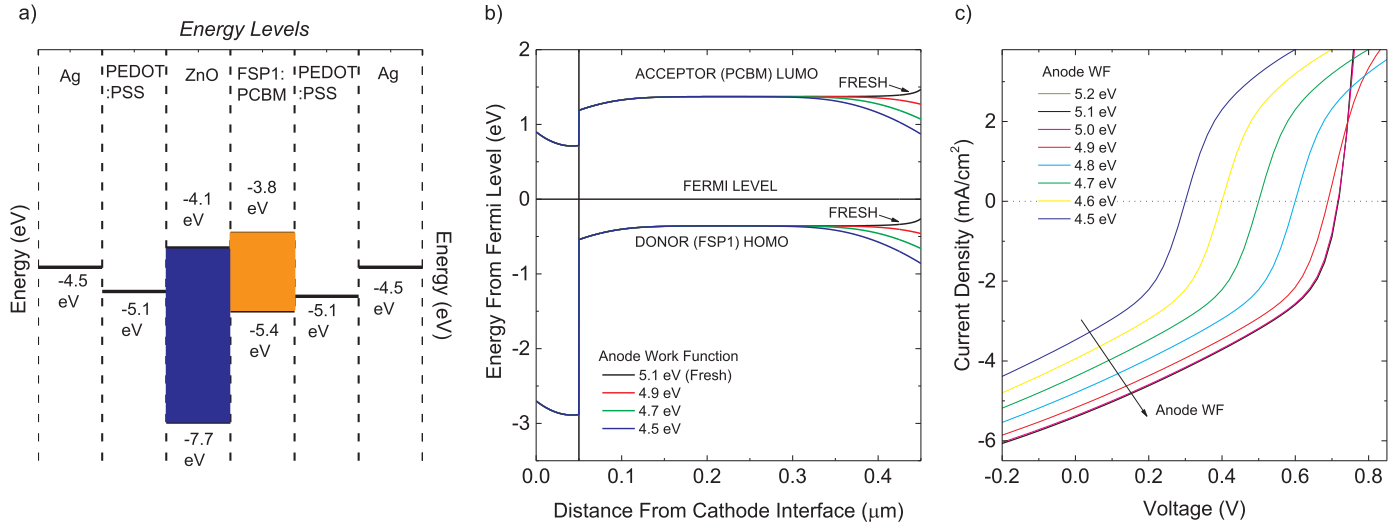

Fig. 8. a) Energy levels, b) band diagram varying the PEDOT:PSS work function of the anode in dark at 0 V, and c) corresponding J-Vs at 1 sun simulated with Silvaco TCAD.

strongly indicates a formation of a depletion region at the anode PEDOT:PSS/active layer interface due to a lowering of the PEDOT:PSS work function of the water degraded samples. This is supported by the appearance of an S-shape in the J-V curve in the water degraded samples that has been widely modelled with a circuit composed of a counter diode in series with the main diode, see inset of Fig. 7 [41,54–56].

In order to corroborate this hypothesis, Fig. 7a shows the fit of the J-V curve under 1 sun illumination AM1.5G of the water-degraded sample (H_2O) with the two-diode circuit of the inset. Fig. 7b shows a

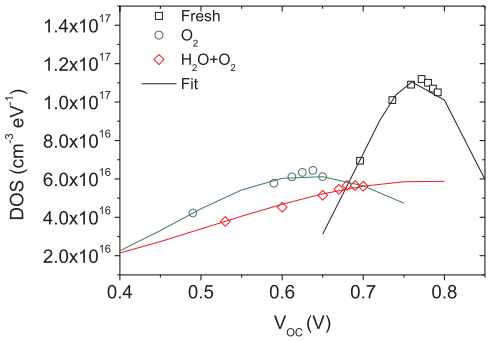

Fig. 9. Gaussian DOS at the LUMO of PCBM obtained by fitting the chemical capacitance extracted from impedance at V_{OC} under different irradiances to Eq. (3).

comparison between resistances obtained from the fit of the J-V curve and Cole-Cole spectra under 1 Sun illumination using the DC and AC circuits, respectively. The forward diode (d1) is associated with the bulk recombination and transport (associated in AC to circuit A of Fig. 5) and the counter diode (d2) is associated to the depletion region formed at the anode responsible for the S-shape (associated in AC to R_3C_3 to circuit B of Fig. 5). The dynamical resistances of the forward and counter diodes are r_{d1} and r_{d2} respectively, given by $r_d = \frac{nV_T}{I_0 \exp\left(\frac{V}{nV_T}\right)}$. It follows that the resistance R_3 obtained from the fit of the Cole-Cole is related to the parallel combination of R_{p2} // r_{d2} obtained from the DC fit. In the same way, the sum of recombination and transport resistances obtained from the fit of the impedance, $R_1 + R_2$, is related to the parallel combination of R_{p1} // r_{d1} of the main diode obtained from the fit of the J-V. Fig. 7b shows a good agreement when comparing R_3 with R_{p2} // r_{d2}, and $R_1 + R_2$ with R_{p1} // r_{d1} supporting the hypothesis of the formation of a depletion zone at the anode.

In order to illustrate the above discussion, Fig. 8 shows the results of a simulation of the band diagram and the corresponding J-V using the commercial software Silvaco TCAD varying the PEDOT:PSS work function of the anode from 5.2 to 4.5 eV. According to semiconductor physics, the Fermi level of the active layer, $E_F \approx 5$ eV (simulations show that the Fermi level of the p-type blend is located 0.36 eV above the HOMO of the PCBM) has to equal the anode work function when both materials are put in contact. As long as the anode work function is equal or above the Fermi level of the blend, i.e., 5 eV or higher (in absolute value), the band diagram remains flat or bends slightly upwards close to the anode, allowing an ohmic contact for holes (fresh sample, Fig. 8b). When the anode work function decreases below the Fermi level of the blend (below 5 eV), the band diagram bends downwards resulting in the formation of an energy barrier for hole extraction that is directly related to the appearance of the S-shape (Figs. 8b and 8c). According to these simulations, we estimate a decrease of 0.3 − 0.4 eV (in the range from 5.2 − 5.1 eV to 4.8 − 4.7 eV) of the PEDOT:PSS work function at the anode for the water degraded sample, in agreement with the appearance of a ~100 nm thick depletion region and a reduction of 0.1 − 0.2 V in V_{OC}.

There is a question remaining unanswered as to whether or not the sample degraded with both water and oxygen (H_2O) also shows the formation of a depletion region at the anode since R_3 and C_3 associated to this sample do not significantly vary with voltage. Moreover, no S-shape appears in the J-V curve, at least in the fourth quadrant. The authors believe that degradation mechanisms due to water and oxygen occur in parallel. In terms of circuit modelling this is represented by two parallel resistances, with total resistance dominated by the smaller of the two. Fig. 6 shows that $R_3 \sim 500\ \Omega$ for the oxygen degraded sample (O_2) while $R_3 \sim 2000\ \Omega$ for the water degraded sample (H_2O) at zero bias. This suggests that when both water and oxygen are present, the degradation process is dominated by oxygen and so is reflected in $R_3 \sim 500\ \Omega$ for the oxygen and water degraded sample ($O_2 + H_2O$). In summary, based on the previous analysis, it is proposed that although the effect of water in the PEDOT:PSS anode interface might be occurring, it is being screened by the oxygen. Moreover, the effect of oxygen in the J-V curve results in a large decrease of the photocurrent, which is manifested in the DC model by a negligible current flowing through the counter diode, and thus, no S-shape can be seen in the water and oxygen degraded sample ($O_2 + H_2O$). This is in agreement with results from previous studies that concluded that R2R inverted structures were more sensitive to oxygen than water [52].

In order to study the effect of the different degradation agents on the active layer, the chemical capacitance has been analysed and related to the density-of-states (DOS). In a first approximation, the DOS g_n of an organic semiconductor is described with a Gaussian function given by Eq. (3) [57–61].

$$g_n(E - E_L) = \frac{N_n}{\sqrt{2\pi\sigma_n}} exp\left[-\frac{(E_L - E)^2}{2\sigma_n^2}\right] \quad (3)$$

where N_n is the total density of states, E_L is the centre of the DOS and σ_n is the width of the DOS associated with the material disorder. Moreover, the dependence of the chemical capacitance on V_{OC} resembles the DOS. Fig. 9 shows the fits of the chemical capacitance extracted from the Cole-Cole spectra under illumination at V_{OC} to Eq. (3).

It is worth noting that whereas the fits shown as solid lines in Fig. 9 may serve as guide lines, the absolute value of σ_n obtained from the fit may present great uncertainty. The increasing trend of σ_n for the (O_2) and ($O_2 + H_2O$) exposed samples (~ 150–250 meV) with respect to the fresh one (~ 65–85 meV), indicates an increasing degree of disorder that might be attributed to the trapping distribution introduced by the oxygen-induced defects. The centre the Gaussian DOS for all samples lies around $E_L = 0.65$–0.85 eV. According to Belmonte *et al.* this value can be viewed as an effective E_{LUMO} for PCBM relative to the Fermi level of holes in the polymer, and it sets the upper limit for V_{OC} [58].

4. Conclusions

We conclude that equivalent circuit modelling of electrical AC and DC measurements is a non-destructive analysis tool to obtain quantitative information about the change in the energy levels, defects density and conductive properties associated with different degradation mechanisms taking place in the device. In this work we have studied degradation of a low cost ITO-free flexible organic solar cell using PEDOT:PSS at both contacts. However, the fact that PEDOT:PSS is highly sensitive to oxygen and water dramatically affects device stability.

The absorption of oxygen in the oxygen degraded samples results in an increased density of defects obtained from Mott-Schottky analysis, which in turn results in a large decrease of the photocurrent. Moreover, the obtained ideality factor indicates that these defects may act as recombination trapping centres.

In order to obtain accurate impedance fits of the degraded samples, an additional parallel element R_3C_3 was added to the main circuit. Furthermore, the different voltage dependence of circuital parameters obtained from the impedance reveal that PEDOT:PSS at the anode interface is being affected differently by oxygen and water. For the oxygen degraded samples (O_2 and $O_2 + H_2O$), R_3 and C_3 are voltage independent suggesting that oxygen is increasing the PEDOT:PSS layer resistivity. However, for the water degraded sample (H_2O), R_3 and C_3 decreases and increases with voltage, respectively. This voltage dependence indicates the appearance of a depletion region at the anode, which is in agreement with previous studies concluding that PEDOT:PSS work function is lowered by the reaction with water. This hypothesis is in good agreement with the appearance of an S-shape in the J-V curve of the water degraded sample (H_2O) that has been successfully modelled with a two-diode circuit.

Acknowledgements

This work has been supported by Programa Estancias Breves José Castillejo (MECD), Comunidad Autónoma de Madrid under Programa de Actividades de I + D SINFOTON S2013/MIT-2790, EU Cost Action MP1307 and Grupos de Excelencia URJC-Banco de Santander 30VCPIGI14. The research leading to these results has also received funding from the European Union Seventh Framework Programme (FP7/2007–2013) under grant agreement n° 609788 and the UK government's Department for Business, Energy and Industrial Strategy.

References

[1] C.J. Brabec, N.S. Sariciftci, J.C. Hummelen, Plastic solar cells, Adv. Mater. 11 (2001) 15–26, http://dx.doi.org/10.1002/1616-3028(200102)11:1<15::AID-ADFM15>3.0.CO;2-A.

[2] S.H. Park, A. Roy, S. Beaupré, S. Cho, N. Coates, J.S. Moon, D. Moses, M. Leclerc, K. Lee, A.J. Heeger, Bulk heterojunction solar cells with internal quantum efficiency approaching 100%, Nat. Photonics 3 (2009) 297–302, http://dx.doi.org/10.1038/nphoton.2009.69.

[3] C.N. Hoth, S.A. Choulis, P. Schilinsky, C.J. Brabec, On the effect of poly(3-hexylthiophene) regioregularity on inkjet printed organic solar cells, J. Mater. Chem. 19 (2009) 5398–5404, http://dx.doi.org/10.1039/B823495G.

[4] F.C. Krebs, All solution roll-to-roll processed polymer solar cells free from indium-tin-oxide and vacuum coating steps, Org. Electron. 10 (2009) 761–768, http://dx.doi.org/10.1016/j.orgel.2009.03.009.

[5] F.C. Krebs, Fabrication and processing of polymer solar cells: a review of printing and coating techniques, Sol. Energy Mater. Sol. Cells 93 (2009) 394–412, http://dx.doi.org/10.1016/j.solmat.2008.10.004.

[6] M.J. Beliatis, K.K. Gandhi, L.J. Rozanski, R. Rhodes, L. McCafferty, M.R. Alenezi, A.S. Alshammari, C.A. Mills, K.D.G. Imalka Jayawardena, S.J. Henley, S. Ravi, P. Silva, Hybrid graphene-metal oxide solution processed electron transport layers for large area high-performance organic photovoltaics, Adv. Mater. 26 (2014) 2078–2083, http://dx.doi.org/10.1002/adma.201304780.

[7] M.A. Green, K. Emery, Y. Hishikawa, W. Warta, E.D. Dunlop, Solar cell efficiency tables (version 49), Progress Photovolt. 25 (2017) 3–13, http://dx.doi.org/10.1002/pip.2855.

[8] M. Jørgensen, K. Norrman, S. Gevorgyan, T. Tromholt, B. Andreasen, F.C. Krebs, Stability of polymer solar cells, Adv. Mater. 24 (2012) 584–612, http://dx.doi.org/10.1002/adma.201104187.

[9] M. Jørgensen, K. Norrman, F.C. Krebs, Stability/degradation of polymer solar cells, Sol. Energy Mater. Sol. Cells 92 (2008) 686–714, http://dx.doi.org/10.1016/j.solmat.2008.01.005.

[10] K. Norrman, M.V. Madsen, S.A. Gevorgyan, F.C. Krebs, Degradation patterns in water and oxygen of an inverted polymer solar cell, J. Am. Chem. Soc. 132 (2010) 16883–16892, http://dx.doi.org/10.1021/ja106299g.

[11] Y. Zhang, H. Yi, A. Iraqi, J. Kingsley, A. Buckley, T. Wang, D.G. Lidzey, Comparative indoor and outdoor stability measurements of polymer based solar cells, Sci. Rep. 7 (2017) 1305, http://dx.doi.org/10.1038/s41598-017-01505-w.

[12] S. Galliano, F. Bella, C. Gerbaldi, M. Falco, G. Viscardi, M. Grätzel, C. Barolo, Photoanode/electrolyte interface stability in aqueous dye-sensitized solar cells, Energy Technol. 5 (2017) 300–311, http://dx.doi.org/10.1002/ente.201600285.

[13] J.R. Swierk, N.S. McCool, T.P. Saunders, G.D. Barber, T.E. Mallouk, Effects of electron trapping and protonation on the efficiency of water-splitting dye-sensitized solar cells, J. Am. Chem. Soc. 136 (2014) 10974–10982, http://dx.doi.org/10.1021/ja5040705.

[14] J. You, L. Meng, T.-B. Song, T.-F. Guo, Y. Yang, W.-H. Chang, Z. Hong, H. Chen, H. Zhou, Q. Chen, Y. Liu, N. De Marco, Y. Yang, Improved air stability of perovskite solar cells via solution-processed metal oxide transport layers, Nat. Nanotechnol. 11 (2016) 75–81, http://dx.doi.org/10.1038/nnano.2015.230.

[15] B. Li, Y. Li, C. Zheng, D. Gao, W. Huang, Advancements in the stability of perovskite solar cells: degradation mechanisms and improvement approaches, RSC Adv. 6 (2016) 38079–38091, http://dx.doi.org/10.1039/C5RA27424A.

[16] F. Bella, G. Griffini, J.P. Correa-Baena, G. Saracco, M. Grätzel, A. Hagfeldt, S. Turri, C. Gerbaldi, Improving efficiency and stability of perovskite solar cells with photocurable fluoropolymers, Science 354 (2016) 203–206, http://dx.doi.org/10.1126/science.aah4046.

[17] D. Pintossi, G. Iannaccone, A. Colombo, F. Bella, M. Välimäki, K.L. Väisänen, J. Hast, M. Levi, C. Gerbaldi, C. Dragonetti, S. Turri, G. Griffini, Luminescent downshifting by photo-induced sol-gel hybrid coatings: accessing multifunctionality on flexible organic photovoltaics via ambient temperature material processing, Adv. Electron. Mater. 2 (11) (2006) 16002, http://dx.doi.org/10.1002/aelm.201600288.

[18] M. Bag, S. Banerjee, R. Faust, D. Venkataraman, Self-healing polymer sealant for encapsulating flexible solar cells, Sol. Energy Mater. Sol. Cells 145 (2016) 418–422, http://dx.doi.org/10.1016/j.solmat.2015.11.004.

[19] A. Rivaton, S. Chambon, M. Manceau, J.L. Gardette, N. Lamaitre, S. Guillerez, Light-induced degradation of the active layer of polymer based solar cells, Polym. Degrad. Stab. 95 (2010) 278–284, http://dx.doi.org/10.1016/j.polymdegradstab.2009.11.021.

[20] M. Manceau, A. Rivaton, J.L. Gardette, S. Guillerez, N. Lemaitre, The mechanism of photo- and thermooxidation of poly(3- hexylthiophene) (p3ht) reconsidered, Polym. Degrad. Stab. 94 (2009) 898–907, http://dx.doi.org/10.1016/j.polymdegradstab.2009.03.005.

[21] J. Schafferhans, A. Baumann, A. Wagenpfahl, C. Deibel, V. Dyakonov, Oxygen doping of P3HT:PCBM blends: influence on trap states charge carrier mobility and solar cell performance, Org. Electron. 11 (2010) 1693–1700, http://dx.doi.org/10.1016/j.orgel.2010.07.016.

[22] M. Reese, A.M. Nardes, B.L. Rupert, R.E. Larsen, D.C. Olson, M.T. Lloyd, S.E. Shaheen, D.S. Ginley, G. Rumbles, N. Kopidakis, Photoinduced degradation of polymer and polymer–fullerene active layers: experiment and theory, Adv. Funct. Mater. 20 (2010) 3476–3483, http://dx.doi.org/10.1002/adfm.201001079.

[23] J.A. Hauch, P. Schilinsky, S.A. Choulis, S. Rajoelson, C.J. Brabec, The impact of water vapor transmission rate on the lifetime of flexible polymer solar cells, Appl. Phys. Lett. 93 (2008) 103306, http://dx.doi.org/10.1063/1.2975185.

[24] E. Voroshazi, B. Verreet, A. Buri, R. Müller, D. Di Nuzzo, P. Heremans, Influence of cathode oxidation via the hole extraction layer in polymer:fullerene solar cells, Org. Electron. 12 (2011) 736–744, http://dx.doi.org/10.1016/j.orgel.2011.01.025.

[25] E. Vitoratos, S. Sakkopoulos, N. Paliatsas, K. Emmanouil, S.A. Choulis, Con- ductivity degradation study of PEDOT:PSS films under heat treatment in helium and atmospheric air, Open J. J. Org. Polym. Mater. 2 (2012) 7–11, http://dx.doi.org/10.4236/ojopm.2012.21002.

[26] V.M. Drakonakis, A. Savva, M. Kokonou, S.A. Choulis, Investigating electrodes degradation in organic photovoltaics through reverse engineering under accelerated humidity lifetime conditions, Sol. Energy Mater. Sol. Cells 130 (2014) 544–550, http://dx.doi.org/10.1016/j.solmat.2014.07.051.

[27] N. Koch, A. Vollmer, A. Elschner, Influence of water on the work function of conducting poly(3,4-ethylenedioxythiophene)/poly(styrenesulfonate), Appl. Phys. Lett. 90 (2007) 043512, http://dx.doi.org/10.1063/1.2435350.

[28] R. Rosch, D.M. Tanenbaum, M. Jørgensen, M. Sealand, M. Barenklau, M. Hermenau, E. Voroshazi, M.T. Lloyd, Y. Galagan, B. Zimmermann, U. Wurfel, M. Hosel, H.F. Dam, S. Gevorgyan, S. Kudret, W. Maes, L. Lutsen, D. Vanderzande, R. Andriessen, G. Teran-Escobar, M. Lira-Cantu, A. Rivaton, G.Y. Uzunoglu, D. Germack, B. Andreasen, M.V. Madsen, K. Norrman, H. Hoppe, F.C. Krebs, Investigation of the degradation mechanisms of a variety of organic photovoltaic devices by combination of imaging techniques — the ISOS-3 inter- laboratory collaboration, Energy Environ. Sci. 5 (2012) 6521–6540, http://dx.doi.org/10.1039/C2EE03508A.

[29] B. Andreasen, D.M. Tanenbaum, M. Hermenau, E. Voroshazi, M.T. Lloyd, Y. Galagan, B. Zimmernann, S. Kudret, W. Maes, L. Lutsen, D. Vanderzande, U. Wurfel, R. Andriessen, R. Rosch, H. Hoppe, G. Teran-Escobar, M. Lira-Cantu, A. Rivaton, G.Y. Uzunoglu, D.S. Germack, M. Hosel, H.F. Dam, M. Jørgensen, S.A. Gevorgyan, M.V. Madsen, E. Bundgaard, F.C. Krebs, K. Norrman, TOF-SIMS investigation of degradation pathways occurring in a variety of organic photovoltaic devices – the ISOS-3 inter-laboratory collaboration, Phys. Chem. Chem. Phys. 14 (33) (2012) 11780–11799, http://dx.doi.org/10.1039/C2CP41787A.

[30] D.M. Tanenbaum, M. Hermenau, E. Voroshazi, M.T. Lloyd, Y. Galagan, B. Zimmermann, M. Hosel, H.F. Dam, M. Jørgensen, S. Kudret, W. Maes, L. Lutsen, D. Vanderzande, U. Wurfel, R. Andriessen, R. Rosch, H. Hoppe, G. Teran-Escobar, M. Lira-Cantu, A. Rivaton, G.Y. Uzunoglu, D. Germack, B. Andreasen, M.V. Madsen, K. Norrman, F.C. Krebs, The ISOS-3 inter-laboratory collaboration focused on the stability of a variety of organic photovoltaic devices, RSC Adv. 2 (3) (2012) 882–893, http://dx.doi.org/10.1039/C1RA00686J.

[31] G. Teran-Escobar, D.M. Tanenbaum, E. Voroshazi, M. Hermenau, K. Norrman, M.T. Lloyd, Y. Galagan, B. Zimmermann, M. Hosel, H.F. Dam, M. Jørgensen, S. Gevorgyan, S. Kudret, W. Maes, L. Lutsen, D. Vanderzande, U. Wurfel, R. Andriessen, R. Rosch, H. Hoppe, A. Rivaton, G.Y. Uzunoglu, D. Germack, B. Andreasen, M.V. Madsen, E. Bundgaard, F.C. Krebs, M. Lira-Cantu, On the stability of a variety of organic photovoltaic devices by IPCE and insitu IPCE analyses – the ISOS-inter-laboratory collaboration, Phys. Chem. Chem. Phys. 14 (33) (2012) 11824–11845, http://dx.doi.org/10.1039/C2CP40821J.

[32] J.E. Carlé, M. Helgesen, N.K. Zawacka, M.V. Madsen, E. Bundgaard, F.C. Krebs, A comparative study of fluorine substituents for enhanced stability of flexible and ITO-free high-performance polymer solar cells, J. Polym. Sci., Part B: Polym. Phys. 52 (2014) 893–899, http://dx.doi.org/10.1002/polb.23505.

[33] A. Guerrero, P. Boix, L.F. Marchesi, T. Ripolles-Sanchis, E.C. Pereira, G. Garcia-Belmonte, Oxygen doping-induced photo-generation loss in P3HT:PCBM solar cells, Sol. Energy Mater. Sol. Cells 100 (2012) 185–191, http://dx.doi.org/10.1016/j.solmat.2012.01.012.

[34] A. Guerrero, S. Chambon, L. Hirsch, G. García-Belmonte, Light-modulated TiOx interlayer dipole and contact activation in organic solar cells cathode, Adv. Funct. Mater. 24 (2014) 6234–6240, http://dx.doi.org/10.1002/adfm.201401233.

[35] I. Mora-Seró, G. García-Belmonte, P.P. Boix, M.A. Váquez, J. Bisquert, Impedance spectroscopy characterisation of highly efficient silicon solar cells under different light illumination intensities, Energy Environ. Sci. 2 (2009) 678–686, http://dx.doi.org/10.1039/B812468J.

[36] T. Ripolles-Sanchís, A. Guerrero, J. Bisquert, G. García-Belmonte, Diffusion-recombination determines collected current and voltage in polymer:fullerene solar cells, J. Phys. Chem. C 116 (2012) 16925–16933, http://dx.doi.org/10.1021/jp305941f.

[37] M.J. Beliatis, M. Helgesen, R. García-Valverde, M. Corazza, B. Roth, J.E. Carlé, M. Jørgensen, F.C. Krebs, S.A. Gevorgyan, Slot-die-coated V2O5 as hole transport layer for flexible organic solar cells and optoelectronic devices, Adv. Eng. Mater. 18 (2016) 1494–1503, http://dx.doi.org/10.1002/adem.201600119.

[38] G.F. Dibb, J.C. Blakesley, F.A. Castro, Environmental stability of organic semiconductors for use in optoelectronic devices (book chapter), in: Werasak Udomkichdecha, Anchalee Mononukul, Thomas Böllinghaus, Jürgen Lexow (eds.), Materials for Energy Infrastructure, Springer, Singapore, Ch. 8, pp. 73–81. ISBN: 978-981-287-724-6.

[39] A. Sundqvist, O.J. Sandberg, M. Nyman, J.-H. Smått, R. Österbacka, Origin of the S-shaped JV curve and the light-soaking issue in inverted organic solar cells, Adv. Energy Mater. 6 (2016) 1502265, http://dx.doi.org/10.1002/aenm.201502265.
[40] B. Ecker, H.J. Egelhaaf, R. Steim, J. Parisi, E. von Hauff, Understanding S-shaped current-voltage characteristics in organic solar cells containing a TiOx interlayer with impedance spectroscopy and equivalent circuit analysis, J. Phys. Chem. C 116 (2012) 16333–16337, http://dx.doi.org/10.1021/jp305206d.
[41] F.A. de Castro, J. Heier, F. Nüesch, R. Hany, Origin of the kink in current-density versus voltage curves and efficiency enhancement of polymer-C60 heterojunction solar cells, IEEE J. Sel. Top. Quantum Electron. 16 (2010) 1690–1699, http://dx.doi.org/10.1109/JSTQE.2010.2040807.
[42] G.A.H. Wetzelaer, M. Kuik, H.T. Nicolai, P.W.M. Blom, Trap-assisted and Langevin-type recombination in organic light-emitting diodes, Phys. Rev. B 83 (2011) 165204, http://dx.doi.org/10.1103/PhysRevB.83.165204.
[43] T. Kirchartz, B.E. Pieters, J. Kirkpatrick, U. Rau, J. Nelson, Recombination via tail states in polythiophene:fullerene solar cells, Phys. Rev. B 83 (2011) 115209, http://dx.doi.org/10.1103/PhysRevB.83.115209.
[44] J.C. Blakesley, D. Neher, Relationship between energetic disorder and open-circuit voltage in bulk heterojunction organic solar cells, Phys. Rev. B 84 (7) (2011) 075210, http://dx.doi.org/10.1103/PhysRevB.84.075210.
[45] T. Kirchartz, F. Deledalle, P.S. Tuladhar, J.R. Durrant, J. Nelson, On the differences between dark and light ideality factor in polymer:fullerene solar cells, J. Phys. Chem. Lett. 4 (14) (2013) 2371–2376, http://dx.doi.org/10.1021/jz4012146.
[46] T. Kirchartz, W. Gong, S.A. Hawks, T. Agostinelli, R.C.I. MacKenzie, Y. Yang, J. Nelson, Sensitivity of the Mott–Schottky analysis in organic solar cells, J. Phys. Chem. C 116 (2012) 7672–7680, http://dx.doi.org/10.1021/jp300397f.
[47] E.H. Rhoderick, R.H. Williams, Metal-semiconductor Contact, Clarendon Press, Oxford, 1988 (ISBN: 0198593368).
[48] J. Bao, I. Shalish, Z. Su, R. Gurwitz, F. Capasso, X. Wang, Z. Ren, Photoinduced oxygen release and persistent photoconductivity in ZnO nanowires, Nanoscale Res. Lett. 6 (2011) 404, http://dx.doi.org/10.1186/1556-276X-6-404.
[49] Y. Jin, J. Wang, B. Sun, J.C. Blakesley, N.C. Greenham, Solution-processed ultraviolet photodetectors based on colloidal ZnO nanoparticles, Nano Lett. 8 (6) (2008) 1649–1653, http://dx.doi.org/10.1021/nl0803702.
[50] G.F.A. Dibb, M.-A. Muth, T. Kirchartz, Sebastian Engmann, Harald Hoppe, G. Gobsch, M. Thelakkat, N. Blouin, S. Tierney, M. Carrasco-Orozco, J.R. Durrant, Jenny Nelson, Influence of doping on charge carrier collection in normal and inverted geometry polymer:fullerene solar cells, Sci. Rep. (2013) 3335, http://dx.doi.org/10.1038/srep03335.
[51] F.F. Stelzl, U. Würfel, Modeling the influence of doping on the performance of bulk heterojunction organic solar cells: one-dimensional effective semiconductor versus two-dimensional donor/acceptor model, Phys. Rev. B 86 (2012) 075315, http://dx.doi.org/10.1103/PhysRevB.86.075315.
[52] F.C. Krebs, S.A. Gevorgyan, J. Alstrup, A roll-to-roll process to flexible polymer solar cells: model studies, manufacture and operational stability studies, J. Mater. Chem. 19 (2009) 5442–5451, http://dx.doi.org/10.1039/b823001c.
[53] S.B. Sapkota, M. Fischer, B. Zimmermann, U. Würfel, Analysis of the degradation mechanism of ITO-free organic solar cells under UV radiation, Sol. Energy Mater. Sol. Cells 121 (2014) 43–48, http://dx.doi.org/10.1016/j.solmat.2013.10.021.
[54] B. Romero, G. del Pozo, B. Arredondo, J.P. Reinhardt, M. Sessler, U. Würfel, Circuital model validation for S-shaped organic solar cells by means of impedance spectroscopy, IEEE J. Photovolt. 5 (2015) 2156–3381, http://dx.doi.org/10.1109/JPHOTOV.2014.2362978.
[55] G. del Pozo, B. Romero, B. Arredondo, Evolution with annealing of solar cell parameters modeling the S-shape of the current–voltage characteristic, Sol. Energy Mater. Sol. Cells 104 (2012) 81–86, http://dx.doi.org/10.1016/j.solmat.2012.04.048.
[56] F.A. Castro, A. Laudani, F.R. Fulginei, A. Salvini, An in-depth analysis of the modelling of organic solar cells using multiple-diode circuits, Sol. Energy 135 (2016) 590–597, http://dx.doi.org/10.1016/j.solener.2016.06.033.
[57] H. Bässler, Charge transport in disordered organic photoconductors a Monte Carlo simulation study, Status Solidi B 175 (1993) 15–297, http://dx.doi.org/10.1002/pssb.2221750102.
[58] G. Garcia-Belmonte, P. Boix, J. Bisquert, M. Sessolo, H.J. Bolink, Simultaneous determination of carrier lifetime and electron density-of-states in P3HT:PCBM organic solar cells under illumination by impedance spectroscopy, Sol. Energy Mater. Sol. Cells 94 (2010) 366–375, http://dx.doi.org/10.1016/j.solmat.2009.10.015.
[59] I.N. Hulea, H.B. Brom, A.J. Houtepen, D. Vanmaekelbergh, J.J. Kelly, E.A. Meulenkamp, Wide energy-window view on the density of states and hole mobility in poly(p-phenylene vinylene), Phys. Rev. Lett. 93 (16) (2004) 166601, http://dx.doi.org/10.1103/PhysRevLett.93.166601.
[60] I. Lange, J.C. Blakesley, J. Frisch, A. Vollmer, N. Koch, D. Neher, Band bending in conjugated polymer layers, Phys. Rev. Lett. 106 (21) (2011) 216402, http://dx.doi.org/10.1103/PhysRevLett.106.216402.
[61] T. Sueyoshi, H. Fukagawa, M. Ono, S. Kera, N. Ueno, Low-density band-gap states in pentacene thin films probed with ultrahigh-sensitivity ultraviolet photoelectron spectroscopy, Appl. Phys. Lett. 95 (18) (2009) 183303, http://dx.doi.org/10.1063/1.3258351.